A reactant-coordinate-based approach to state-to-state differential cross sections for tetratomic reactions

Bin Zhao, Zhigang Sun, and Hua Guo

Citation: The Journal of Chemical Physics **145**, 184106 (2016); doi: 10.1063/1.4966966
View online: https://doi.org/10.1063/1.4966966
View Table of Contents: http://aip.scitation.org/toc/jcp/145/18
Published by the American Institute of Physics

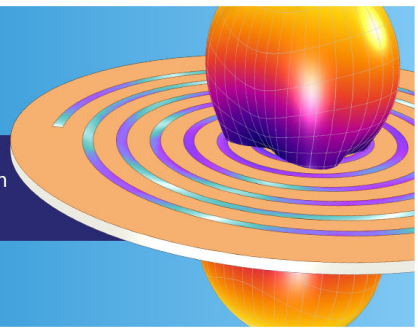

A reactant-coordinate-based approach to state-to-state differential cross sections for tetratomic reactions

Bin Zhao,[1] Zhigang Sun,[2,a)] and Hua Guo[1,a)]
[1]*Department of Chemistry and Chemical Biology, University of New Mexico, Albuquerque, New Mexico 87131, USA*
[2]*State Key Laboratory of Molecular Reaction Dynamics and Center for Theoretical and Computational Chemistry, Dalian Institute of Chemical Physics, Chinese Academy of Sciences, Dalian 116023, China*

(Received 28 September 2016; accepted 21 October 2016; published online 9 November 2016)

A new algorithm is proposed to compute quantum mechanically state-to-state differential cross sections for reactions involving four atoms in full dimensionality. This algorithm, which is based on the propagation of an initial state specific wave packet exclusively in reactant coordinates, extracts the *S*-matrix elements in the product channel by first interpolating the time-dependent wave packet using a collocation method at selected time intervals on the product coordinate grid and then projecting out the contributions of all final product states. This approach is efficient and accurate, particularly for reactions that are dominated by a product well or long-range interactions. Validation of this approach is demonstrated for the $H_2 + OH \rightarrow H + H_2O$ reaction. *Published by AIP Publishing.* [http://dx.doi.org/10.1063/1.4966966]

I. INTRODUCTION

Thanks to recent advances in the experimental measurement of state-to-state differential cross sections (DCSs) for bimolecular reactive scattering processes,[1–4] there has been much renewed interest in developing new theoretical methods and models to understand such detailed experimental observations.[5–11] Many of the recent advances in theoretical reaction dynamics have been made beyond atom-diatom reactions and they start to help us understand the richer chemistry in polyatomic reactive systems. The progress has partly been stimulated by the availability of high-dimensional accurate reactive potential energy surfaces (PESs) based on large numbers of *ab initio* points.[7,9,12–14] Technically, these new theoretical studies were almost exclusively based on solving the time-dependent Schrödinger equation or its equivalent because an initial value problem is much easier to handle numerically than a boundary condition problem of the time-independent form of the Schrödinger equation.[15] Despite these advances, it is still very challenging to compute quantum DCSs in full dimensionality for reactions involving more than three atoms. Up to now, quantum DCS calculations have been restricted to the simplest direct tetratomic reaction with a single barrier, namely $H_2 + OH \leftrightarrow H + H_2O$ and its isotopologues.[16–21]

Quantum mechanically, the DCS at a particular energy is related to a coherent sum of the reactive scattering matrix (*S*-matrix) elements over partial waves.[15] The problem for computing *S*-matrix elements is mostly associated with the so-called "coordinate problem," namely the difficulty in defining a coordinate system that is optimal for both the reactant and product arrangement channels.[6,10] Reactant coordinates are preferred for the definition of the initial state, but product coordinates are natural for extracting the *S*-matrix elements. Currently, there are four major strategies in mitigating this vexing coordinate problem. The first approach uses the product Jacobi coordinates in propagation.[22–28] While straightforward in determining the *S*-matrix elements in the product asymptote, it is necessary for such product-coordinate-based (PCB) methods to define the initial wave packet, which may require a very large grid in the product coordinates, particularly for large *J* partial waves. For this reason, the PCB strategy is not considered as the most efficient and is now seldom used by practitioners. The second approach is based on propagation in the reactant Jacobi coordinates, but such a reactant-coordinate-based (RCB) method requires special attention in how to extract the *S*-matrix elements.[29–32] One effective way is to define a set of intermediate coordinates, to which both the propagating wave packet and product state wavefunctions are transformed.[29,31,32] However, such an approach requires a very large memory space to store all the product states in the intermediate coordinates, which becomes difficult for tetratomic systems. The third strategy is the so-called reactant-product-decoupling (RPD) scheme, in which a part of the propagating wave packet entering the product channel is removed by an absorbing potential and propagated in the product coordinates.[33–37] This RPD approach has been very successful. In fact, this is the method used to compute the existing quantum DCSs for the $H_2 + OH \leftrightarrow H + H_2O$ reaction and its isotopologues.[16–21] However, it might encounter problems if the product channel is dominated by a post-transition state well or long-range interactions, which necessitate trapped states such as in the case of $F + H_2O \rightarrow HF + OH$ [38–40] and $O(^3P) + H_2O \rightarrow OH + OH$ reactions.[41–43] In addition, the RPD method also encounters difficulties for reactions with low product

a)Authors to whom correspondence should be addressed. Electronic addresses: zsun@dicp.ac.cn and hguo@unm.edu

translational energies.[44] Finally, a new approach based on transition-state wave packets (TSWPs) essentially eliminates the coordinate problem, as separated propagations of the TSWPs into the reactant and product channels can be readily carried out in the appropriate coordinates.[45–50] Different from the above three methods that produce a single column of the S-matrix, the TSWP approach generates the entire S-matrix. A potential shortcoming of the TSWP approach is the slow convergence with respect to the number of TSWPs, which can be quite large for reactions involving heavy atoms or loose barriers.[51,52]

In this work, we present a new RCB method for computing S-matrix elements for tetratomic systems. It involves the interpolation of the time-dependent wave packet, using a collocation method at selected time intervals, on the product grid that naturally defines the product asymptotic states. This approach has been successfully demonstrated in atom-diatom reactions.[30] Here, we generalize this method to the calculation of the S-matrix elements and corresponding DCSs for tetratomic systems using the $H_2 + OH \rightarrow H + H_2O$ reaction as an example. Despite several reports on the DCSs of its isotopically substituted reactions,[16–20] a full-dimensional quantum calculation of DCSs for this reaction has only appeared after the submission of this manuscript, but using the RPD method.[21]

II. THEORY

A. Hamiltonian

In the RCB treatment of a tetratomic reaction at the state-to-state level, the wave packet is propagated exclusively in the reactant coordinates. Nonetheless, the product coordinates also need to be defined because they are required to define the product states used for computing the S-matrix elements. As shown in Fig. 1, the AB + CD and A + BCD arrangements are best described by the corresponding Jacobi coordinates denoted as $(R, r_1, r_2, \theta_1, \theta_2, \varphi)$ and $(R', r_1', r_2', \theta_1', \theta_2', \varphi')$, respectively.[25,26,28,37] In both coordinate systems, the z-axis of the body-fixed (BF) frame is chosen along the $\boldsymbol{R}$ and $\boldsymbol{R}'$ vectors, respectively, with the vectors $\boldsymbol{r}_1$ and $\boldsymbol{r}_1'$ in the corresponding x-z planes. The triangle consisting of A, B, and the CD center-of-mass (COM) forms a common plane for the two coordinate systems, with $\boldsymbol{r}_2$ and $\boldsymbol{r}_2'$ representing the same vector.

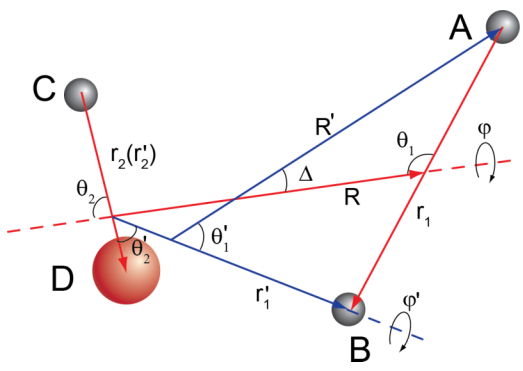

FIG. 1. The reactant AB + CD Jacobi coordinates $(R, r_1, r_2, \theta_1, \theta_2, \varphi)$ and the product A + BCD Jacobi coordinates $(R', r_1', r_2', \theta_1', \theta_2', \varphi')$ for tetra-atomic reactions. The angle between the two BF z-axes $\hat{\boldsymbol{R}}$ and $\hat{\boldsymbol{R}}'$ is denoted as Δ.

For a diatom-diatom reaction, only the Hamiltonian for the AB + CD arrangement is explicitly required in the propagation ($\hbar = 1$ hereafter),

$$\hat{H} = -\frac{1}{2\mu}\frac{\partial^2}{\partial R^2} + \frac{(\hat{J}_{tot} - \hat{j}_{12})^2}{2\mu R^2} + \sum_{k=1}^{2}\left[\hat{h}_k(r_k) + \frac{\hat{j}_k^2}{2\mu_k r_k^2}\right] + V(R, r_1, r_2, \theta_1, \theta_2, \varphi), \quad (1)$$

where μ_1 and μ_2 are the reduced masses for AB and CD, and μ the reduced mass between the AB and CD COMs. The rotational angular momentum operators of AB and CD, $\hat{j}_1$ and $\hat{j}_2$, are coupled to form $\hat{j}_{12}$, and $\hat{J}_{tot}$ is the conserved total angular momentum operator of the system. The reference vibrational Hamiltonians $\hat{h}_k(r_k)$ for the two diatoms are defined as

$$\hat{h}_k(r_k) = -\frac{1}{2\mu_k}\frac{\partial^2}{\partial r_k^2} + V_k(r_k), \quad (k = 1, 2), \quad (2)$$

where $V_k(r_k)$ are the one-dimensional reference potentials, which have been removed from the overall PES in V of Eq. (1). The Hamiltonian for the product arrangement can be similarly defined and has been described in previous publications.[18,48,53] Although the discretization scheme for the wave function in the BF bases has been described in previous publications,[18,48,53] it is nevertheless included here for a complete description of the interpolation scheme and the reactant/product wave packets.

The wave functions are expressed in the BF frame by using following bases:

$$\Psi^{J_{tot}M\varepsilon}(\boldsymbol{R}, \boldsymbol{r}_1, \boldsymbol{r}_2, t) = \sum_{n,\upsilon,j,K} F_{n\upsilon jK}^{J_{tot}M\varepsilon}(t) u_n^{\upsilon_1}(R)\phi_{\upsilon_1}^1(r_1) \times \phi_{\upsilon_2}^2(r_2) y_{jK}^{J_{tot}M\varepsilon}(\hat{R}, \hat{r}_1, \hat{r}_2), \quad (3)$$

where M is the quantum number for the projection of the J_{tot} onto the Z-axis of the space-fixed (SF) frame. υ is a composite index denoting the two vibrational quantum numbers, υ_1 and υ_2 of the two diatomic reactants. The vibrational basis functions $\phi_{\upsilon_i}^i(r_i)$ are the eigenfunctions of the reference vibrational Hamiltonians $\hat{h}_i(r_i)$ and they are represented by the potential-optimized discrete variable representation (PODVR) basis functions.[54,55] The translational basis $u_n^{\upsilon_1}(R)$ along R is defined differently in the asymptotic and interaction regions[56]

$$u_n^{\upsilon_1}(R) = \begin{cases} \sqrt{\frac{2}{L_{asy}}}\sin\frac{n\pi(R - R_1)}{L_{asy}}, \upsilon_1 \le \upsilon_{asy}, R \in (R_1, R_3) \\ \sqrt{\frac{2}{L_{int}}}\sin\frac{n\pi(R - R_1)}{L_{int}}, \upsilon_1 > \upsilon_{asy}, R \in (R_1, R_2) \end{cases}, \quad (4)$$

in an L-shaped scheme.[57] The R coordinate range (R_1, R_3) is divided into the asymptotic and interaction regions at the intermediate point $R_2 = R_1 + N_1^R\Delta_R$, $\Delta_R = (R_3 - R_1)/N_2^R$, and $L_{asy} = R_3 - R_1$ and $L_{int} = R_2 - R_1$ are the lengths of the two regions, respectively. υ_{asy} is chosen to include all energetically open vibrational channels plus a few closed ones. The second composite index j denotes (j_1, j_2, j_{12}), ε

is the parity of the system defined as $\varepsilon = (-1)^{j_1+j_2+l}$ with l being the quantum number for the orbital angular momentum operator $\hat{l} = \hat{J}_{tot} - \hat{j}_{12}$. The parity-adapted BF rotational basis $y_{jK}^{J_{tot}M\varepsilon}(\hat{R},\hat{r}_1,\hat{r}_2)$ is given as

$$y_{jK}^{J_{tot}M\varepsilon}(\hat{R},\hat{r}_1,\hat{r}_2) = \sqrt{\frac{2J_{tot}+1}{8\pi(1+\delta_{K0})}}\,[D_{K,M}^{J_{tot}*}(\alpha,\beta,\gamma)Y_{j_1j_2}^{j_{12}K}(\theta_1,\theta_2,\varphi) + \varepsilon(-1)^{j_1+j_2+j_{12}+J_{tot}}D_{-K,M}^{J_{tot}*}(\alpha,\beta,\gamma)\,Y_{j_1j_2}^{j_{12}-K}(\theta_1,\theta_2,\varphi)], \tag{5}$$

where $D_{K,M}^{J_{tot}}(\alpha,\beta,\gamma)$ is the Wigner matrix[58] that rotates the SF frame to the BF frame by three Euler angles (α,β,γ). The restriction, $\varepsilon(-1)^{j_1+j_2+j_{12}+J_{tot}} = 1$, for $K = 0$ partitions the rotational basis set into even and odd parities. Although the basis functions have the same formal form in Eq. (5) for both the reactant and product wave functions, $Y_{j_1j_2}^{j_{12}K}(\theta_1,\theta_2,\varphi)$ is defined differently for the reactant and product arrangements. The rotational basis $Y_{j_1j_2}^{j_{12}K}(\theta_1,\theta_2,\varphi)$ in the AB + CD arrangement is given by[59]

$$Y_{j_1j_2}^{j_{12}K}(\theta_1,\theta_2,\varphi) = \sum_{m_1}\langle j_1m_1j_2K-m_1\,|\,j_{12}K\rangle \times y_{j_1m_1}(\theta_1,0)\,y_{j_2K-m_1}(\theta_2,\varphi), \tag{6}$$

where y_{jm} is the spherical harmonics and $\langle j_1m_1j_2K-m_1\,|\,j_{12}K\rangle$ is the Clebsch-Gordan coefficient[58] that combines the two spherical harmonics to form the coupled rotational basis. On the other hand, the rotational basis in the A + BCD arrangement, denoted with primes, is given by[60]

$$Y_{j'_1j'_2}^{j'_{12}K'}(\theta'_1,\theta'_2,\varphi') = \sum_{m'} D_{K'm'}^{j'_{12}*}(0,\theta'_1,\varphi')\sqrt{\frac{2j'_1+1}{4\pi}} \times \left\langle j'_2m'j'_10\,|\,j'_{12}m'\right\rangle y_{j_2m'}(\theta'_2,0), \tag{7}$$

where the Wigner matrix $D_{K'm}^{j'_{12}*}(0,\theta'_1,\varphi')$ rotates the BF frame to the molecular-fixed (MF) frame (the z axis of this frame lies along vector $\boldsymbol{r}'_1$) by the Euler angles $(0,\theta'_1,\varphi')$.

B. Extraction of state-to-state S-matrix elements

The state-to-state S-matrix element between the initial reactant state i and final product state f is obtained by a Fourier transform of the time-dependent cross-correlation function[61]

$$S_{pf\leftarrow ri}(E) = \frac{1}{2\pi\eta_f^{-*}(E)\eta_i^{+}(E)}\int_0^\infty e^{iEt}\left\langle\Phi_f^p\right|e^{-iHt}\left|\Phi_i^r\right\rangle dt = \frac{1}{2\pi\eta_f^{-*}(E)\eta_i^{+}(E)}\left\langle\Psi_f^p(E)\,|\,\Psi_i^r(E)\right\rangle, \tag{8}$$

where $\left|\Psi_i^r(E)\right\rangle = \int_0^\infty e^{iEt}\left|\Phi_i^r(t)\right\rangle dt = \int_0^\infty e^{iEt}e^{-iHt}\left|\Phi_i^r\right\rangle dt$ transforms the time-dependent wave packet ($\left|\Phi_i^r(t)\right\rangle \equiv e^{-iHt}\left|\Phi_i^r\right\rangle$) into the energy domain and the $\eta_i^+(E)$ and $\eta_f^-(E)$ are the energy normalization factors of the state-specific reactant and product wave packets ($\left|\Phi_i^r\right\rangle$ and $\left|\Phi_f^p\right\rangle$). These wave packets are best defined in their corresponding coordinate systems, i.e., the AB + CD and A + BCD Jacobi coordinates, respectively. In order to calculate the state-to-state S-matrix element, they need to be transformed into a common set of coordinates to facilitate the projection.

C. Interpolation scheme and product state projection

The transformation between different coordinate systems in the RCB method can be performed either through interpolation[30,61] or using the intermediate coordinate method.[29,31,32] Previously, we have implemented the latter by projecting the Fourier transformed time-dependent wave packet onto the final product states in a set of intermediate coordinates,[29,31] which includes the product-channel scattering coordinate R'. This scheme enables the expression of each product state wave packet in a product form with a delta function in the scattering coordinate that defines the projection plane ($R' = R_p^\infty$). To facilitate the projection, all product state wave packets in the intermediate coordinates have to be stored in the internal memory or on the disk. For tetratomic systems with $J_{tot} > 0$, the massive number of product states with all K' values renders this scheme difficult.

To balance the needs between CPU and data storage, we choose here an interpolation scheme based on a collocation method[62] to extract S-matrix elements. To this end, the time-dependent wave packet is interpolated directly in the product coordinates while the product state wave packets are stored in a direct product form, requiring little memory. The interpolation method has a much less demand on memory, albeit at the expense of the CPU time. To cut down the CPU costs, the interpolation is performed not in every propagation step, but at selected time intervals. The Fourier transform of the time correlation function with a larger time step (Eq. (8)) only reduces the energy span, with no impact on the energy resolution, which is determined by the total propagation length. This idea is similar to the higher-order split-operator method in a time-dependent wave packet calculation.[63,64]

The interpolation of the time-dependent wave packet is performed on a projection plane located at $R' = R_p^\infty$ in the product Jacobi coordinates. This simplifies the expression of the product state wave packets to the product of a delta function in R' and internal ro-vibrational states of the products (see below). The vibrational wave functions can be efficiently represented by a small number of PODVR basis functions. While for the angular degrees of freedom $(\theta'_1,\theta'_2,\varphi')$, the number of rotational bases is also not very large. The interpolation is similar to the transformation of the time-dependent wave packet to the product Jacobi coordinates. The details of the transformation can be found in previous work,[17,36] and here only a brief outline is provided. In particular, the time-dependent wave packet is interpolated on the product grid points without transforming to the corresponding product basis sets. Specifically, the transformation requires a mapping of the six-dimensional time-dependent wave packet $\Phi(R,r_1,r_2,\theta_1,\theta_2,\varphi;t)$ onto the five-dimensional product grids $(r'_1,r'_2,\theta'_1,\theta'_2,\varphi';R_p^\infty)$, in which the scattering coordinate R' is fixed and r'_2 is identical to the reactant r_2 coordinate. It is worth noting here that the product (θ'_2,φ') grid at fixed $(r'_1,\theta'_1;R_p^\infty)$ has a

one-to-one match to the reactant (θ_2,φ) grid at fixed procedure can be divided into the following steps. The time-dependent wave packet is first interpolated on the reactant (R,r_1,θ_1) grid that is determined by the corresponding $(r_1',\theta_1';R_p^\infty)$ grid with the corresponding basis functions $u_n^{v_1}(R)$ and $\phi_{v_1}^1(r_1)$ in Eq. (3) and $y_{j_1m_1}(\theta_1,0)$ in Eq. (6). At a fixed $(r_1',\theta_1';R_p^\infty)$ grid point, the wave packet on all the reactant (θ_2,φ) grid points determined by the corresponding product (θ_2',φ') grid points is obtained by interpolation using the rotational basis functions $y_{j_2K-m_1}(\theta_2,\varphi)$ in Eq. (6). This procedure is efficient because it avoids duplicating the interpolation on the (R,r_1,θ_1) grid points at all the (θ_2',φ') grid points. For nonzero J_{tot} with multiple helicity quantum number K values, all the K components are explicitly calculated and Fourier transformed to the energy domain before they are rotated from the R to R' axes in the BF frames.[29] Finally, they are converted to the basis representation in a product arrangement by a collocation method along the r_1' coordinate and by transformation matrices in other coordinates.[62] To this end, the projection of the propagating wave packet onto all the final product states can be readily evaluated by evaluating the coefficients $\left\langle \Psi^p_{J'v'l'}(E;R_p^\infty)\right|\left.\Psi^r_{v_0j_0l_0}(E;R_p^\infty)\right\rangle$, the description of which will become clear in Sec. II D.

D. Initial wave packet and final state analysis

The initial wave packet in the reactant asymptote is conveniently expressed as a product of the reactant internal state wave function $\psi_i^r(r_1,r_2,\theta_1,\theta_2,\varphi)$ and a Gaussian-shaped wave packet $G(R)$ along the R coordinate,

$$|\Phi_i^r\rangle = \sqrt{\frac{2J_{tot}+1}{8\pi(1+\delta_{K_0 0})}} D^{J_{tot}*}_{K_0,M}(\alpha,\beta,\gamma)G(R) \times \psi_i^r(r_1,r_2,\theta_1,\theta_2,\varphi). \quad (9)$$

The parity ε here is dropped for clarity. The Gaussian-shaped wave packet $G(R)$ is given as follows:

$$G(R) = \left(\frac{1}{\pi\delta^2}\right)^{1/4} \exp\left[-\frac{(R-R_0)^2}{2\delta^2}\right] e^{-ik_0R}, \quad (10)$$

where R_0, δ, and k_0 are the central position, width, and mean translational momentum of the initial wave packet, respectively. The internal wavefunction $\psi_i^r(r_1,r_2,\theta_1,\theta_2,\varphi)$ of the ro-vibrational states of AB and CD reactants assumes the following form:

$$\psi_i^r = \psi^K_{v_0j_0} = \psi^K_{v_{10}v_{20}j_{10}j_{20}j_{120}}(r_1,r_2,\theta_1,\theta_2,\varphi) = \tilde\phi^1_{v_{10}j_{10}}(r_1)\tilde\phi^2_{v_{20}j_{20}}(r_2)Y^{j_{120}K}_{j_{10}j_{20}}(\theta_1,\theta_2,\varphi), \quad (11)$$

where $(v_{10}j_{10})$ and $(v_{20}j_{20})$ are the vibrational and rotational quantum numbers of the ro-vibrational states, $\tilde\phi^1_{v_{10}j_{10}}(r_1)$ and $\tilde\phi^2_{v_{20}j_{20}}(r_2)$, of the AB and CD diatomic molecules, respectively, and the quantum number j_{120} denotes the relative orientation of the two reactants.

The final product state $\left|\Phi_f^p\right\rangle$ is defined on the projection plane defined at $R'=R_p^\infty$ and the internal ro-vibrational wavefunction of the BCD product (ψ_f^p) is defined as follows:

$$\psi_f^p = \tilde\phi_{J'v'K'}(\hat R',\boldsymbol{r}_1',\boldsymbol{r}_2') = \sum_{v_1',v_2',j_1',j_2'} C^{v'}_{v_1'v_2'j_1'j_2'}\phi_{v_1'}(r_1')\phi_{v_2'}(r_2')y^{J_{tot}M\varepsilon}_{j_1'j_2'J'K'}(\hat R',\hat r_1',\hat r_2'), \quad (12)$$

where J' (or j_{12}') and v' denote the rotational and vibrational quantum numbers of the BCD product.

As discussed in the literature,[23,35,61] the SF frame is advantageous to define the initial state wave packet and perform final asymptotic analysis by avoiding the long-ranged Coriolis coupling in the BF frame, as the orbital angular momentum $\hat l^2=(\hat J_{tot}-\hat j_{12})^2$ is diagonal in the SF frame in the absence of interaction potential. However, the wave packet needs to be transformed to the BF frame before the propagation and the details of the transformation can be found in our previous work.[32] The energy normalizing factors $\eta^+_{v_0j_0l_0}(E)$ and $\eta^-_{J'v'l'}(E)$ of the initial and final state wave packets have also been discussed in our previous work[32] and thus are not given here.

The state-to-state S-matrix elements in the SF frame are now expressed as

$$S^{J_{tot}\varepsilon}_{J'v'l'\leftarrow v_0j_0l_0}(E) = \frac{1}{2\pi\eta^{-*}_{J'v'l'}(E)\eta^+_{v_0j_0l_0}(E)} \times \left\langle \Psi^p_{J'v'l'}(E;R_p^\infty)\right|\left.\Psi^r_{v_0j_0l_0}(E;R_p^\infty)\right\rangle. \quad (13)$$

Finally, a standard transformation is used to convert the S-matrix elements from the SF frame to the BF helicity representation by[15]

$$S^{J_{tot}\varepsilon}_{J'v'K'\leftarrow v_0j_0K_0} = \sum_{l'l_0} i^{l_0-l'}\sqrt{\frac{2l'+l}{2J_{tot}+1}}\langle J'K'l'0|\ J_{tot}K'\rangle \times S^{J_{tot}\varepsilon}_{J'v'l'\leftarrow v_0j_0l_0}\sqrt{\frac{2l_0+1}{2J_{tot}+1}} \times \langle j_{120}K_0l_00\,|J_{tot}K_0\rangle. \quad (14)$$

The state-to-state ICS is given by the sum of the contributions of all partial waves,

$$\sigma_{J'v'\leftarrow v_0j_0}(E) = \frac{\pi}{(2j_{10}+1)(2j_{20}+1)k^2_{v_0j_0}}\sum_\varepsilon\sum_{K'}\sum_{K_0}\sum_{J_{tot}} \times(2J_{tot}+1)\left|S^{J_{tot}\varepsilon}_{J'v'K'\leftarrow v_0j_0K_0}(E)\right|^2, \quad (15)$$

and the state-to-state DCS into a solid angle (Ω) is given by the following equation:

$$\frac{d\sigma_{J'v'\leftarrow v_0j_0}(\vartheta,E)}{d\Omega} = \frac{1}{(2j_{10}+1)(2j_{20}+1)}\sum_\varepsilon\sum_{K'}\sum_{K_0}\left|\sum_{J_{tot}}\frac{1}{2ik^2_{v_0j_0}}(2J_{tot}+1)d^{J_{tot}}_{K',K_0}(\vartheta)S^{J_{tot}\varepsilon}_{J'v'K'\leftarrow v_0j_0K_0}(E)\right|^2, \quad (16)$$

where ϑ is the scattering angle between the direction of the incoming reactant CD and outgoing product BCD in the center of mass frame, and $d^{J_{tot}}_{K',K_0}(\vartheta)$ is the reduced rotational matrix.[58]

III. RESULTS AND DISCUSSION

The $H_2 + OH \rightarrow H + H_2O$ reaction and its isotopologues are considered as a prototypic diatom-diatom reaction, and their state-to-state dynamics have been subjected to both experimental[16,17,65] and theoretical studies.[16–18,20,21,36,37,48,49,53,66–70] Most notably, the $D_2 + OH \rightarrow D + HOD$ and $HD + OH \rightarrow D + H_2O$ reactions have been investigated using crossed molecular beam techniques by the Davis[65] and Yang groups.[16,17] It was found that the products are scattered backward relative to the OH direction, suggesting a straightforward direct rebound mechanism. These experimental observations have been reproduced by Zhang and co-workers[16–18] and by us[20] using full-dimensional quantum mechanical methods based on the RPD approach. As mentioned above, there is only one report on the full-dimensional quantum DCS for the $H_2 + OH \rightarrow H + H_2O$ reaction using the RPD method.[21]

All the calculations reported here were performed on the CXXZ PES of the H_3O system[71] using the second-order splitting operator method[72] for the time propagation. We note in passing that this method is also amenable to the Chebyshev propagator[73] as well. Only the ground ro-vibrational states of H_2 and OH reactants are considered. In Fig. 2, the norm of the interpolated wave packet for $J_{tot} = 0$ is plotted against the propagation time. The wave packet reaches the projection plane only after ~2500 a.u. and its norm on the projection plane gradually decays after it reaches its maximum around 4000 a.u. This suggests that the interpolation needs to be performed only after 2500 a.u. The parameters used in the calculations are listed in Table I.

As a necessary condition, the total reaction probabilities obtained by summing up all the state-to-state (S2S) reaction probabilities should match the ones obtained by a flux operator. This is what we can observe in Fig. 3 for the total reaction probabilities at $J_{tot} = 0, 10, 20, 30$. They agree very well with each other for the four J_{tot} values considered here and consequently support the validity of the RCB method. For $J_{tot} = 0$, the threshold of the total reaction probability lies near the collision energy of 0.15 eV. With the increase of J_{tot}, the threshold gradually increases to a higher collision energy due to the centrifugal potential. For $J_{tot} = 30$, the threshold exceeds the collision energy of 0.4 eV, which suggests that J_{tot} values up to 30 are sufficient to converge to the state-to-state DCS for the collision energy of $Ec = 0.4$ eV.

As alluded to above, the interpolation on the product grid is rather time consuming. The scaling of the wave packet propagation is $(N_R + N_{r_1} + N_{r_2} + N_{\theta_1} + N_{\theta_2} + N_\varphi) N_R N_{r_1} N_{r_2} N_{\theta_1} N_{\theta_2} N_\varphi$, while that for interpolation is $(N_R N_{r_1} + N_{\theta_2'} N_\varphi') N_{r_1'} N_{\theta_1'} N_{r_2} N_{\theta_1} N_{\theta_2} N_\varphi$, where the numbers of grid points are labeled by the subscript of the corresponding degrees of freedom. The first term in the latter expression stems from the interpolation of the propagating wave packet on the $(r_1', \theta_1'; R_p^\infty)$ grid while the second term is for the

TABLE I. Parameters used in the calculations (atomic units are used if not otherwise stated).

Initial wave packet			
R_0	11.0		
δ	0.35		
k_0	$k_0 = \sqrt{2E_0\mu}$ with $E_0 = 0.3$ eV		
Parameters for reactant coordinates		Parameters for product coordinates	
R	(1.0,14.0), $N_1^R = 80$, $N_2^R = 128$		
r_1	(0.7,12.0), $\upsilon_1^{int} = 64$, $\upsilon_1^{asy} = 8$	r_1'	(0.7,5.0), $\upsilon_1' = 8$
r_2	(0.7,5.0), $\upsilon_2 = 4$	r_2'	(0.7,5.0), $\upsilon_2' = 4$
j_1	(0,96), even symmetry	j_2'	(0,20)
j_2	(0,20)	j_{12}'	(0,28)
Total propagation time/time step: 8000/10 Partial waves: $J_{tot} = 0$-30 Helicity quantum numbers			
K	(0-6)	K'	(0-13)
Absorbing potential			
	C	x_s	x_e	n
R	0.045	12.0	14.0	1.5
r_1	0.050	10.0	12.0	1.5
Projection plane: $R_P^\infty = 8.0$ Flux plane: $r_1^{flux} = 6.0$				

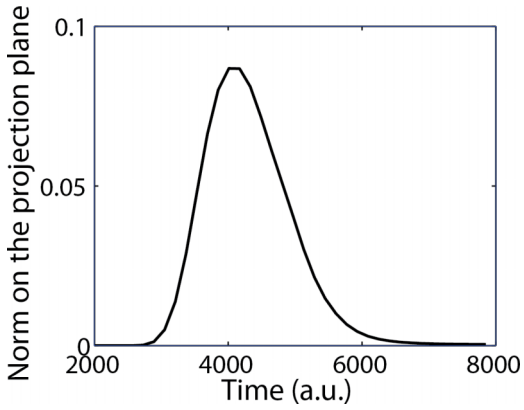

FIG. 2. Norm of the interpolated wave packet represented on the projection plane for $J_{tot} = 0$ as a function of the propagation time.

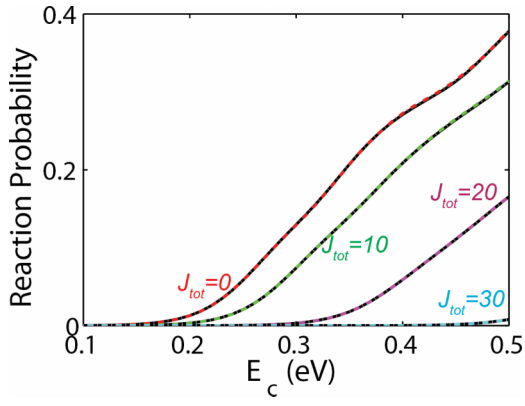

FIG. 3. Comparison of the total reaction probabilities obtained by summing up all the state-to-state (S2S) reaction probabilities (solid) and the flux operator method (dashed) at four selected partial waves of $J_{tot} = 0, 10, 20, 30$.

interpolation on the (θ_2', φ') grid. To get some idea on the relative computational costs of these two operations, the subroutines for performing a single interpolation and one step propagation are timed. For the case of $J_{tot} = 0$, the interpolation takes 13-14 s against 4-5 s for propagation on a single node with four Intel® Xeon® CPUs of E7-4809 v3 @ 2.00 GHz. While for $J_{tot} = 20$ with 6 K-blocks, the interpolation takes 121-122 s against 58-59 s for propagation. Hence, each interpolation is about twice as costly as a propagation step.

Fortunately, it is not necessary to perform the interpolation at every propagation step. To determine the largest allowed time interval for interpolation, the total reaction probabilities obtained by summing up all the S2S reaction probabilities are compared for different intervals ($N = 8, 16, 24$, and 32) in Fig. 4 using the current parameters in Table I. The results obtained by $N = 8$ and 16 agree with each other quite well, while those obtained by $N = 24$ and 32 contain some errors, especially at the low energy part. Thus, an N of 16 was used in the present calculations. This idea is similar to the multi-step RPD (MRPD) method,[74] in which the source term is extracted and fed at every N propagation steps. Between the intervals, the extracted wave packet is propagated in the product channel without the absorbing potential. As a result, N needs to be sufficiently small to prevent the wave function reaching the end of the grid. On the other hand, the interpolation in our RCB method is independent of the application of the absorbing potential on the wave function. As a result, N is determined solely by the energy range of the initial wave packet, which is an energy-time relation of the Fourier transform.

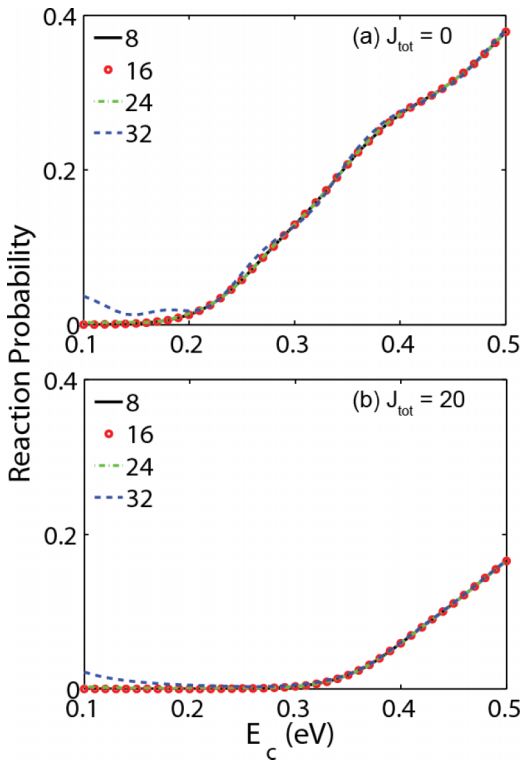

FIG. 4. Total reaction probabilities obtained by summing up all the state-to-state (S2S) reaction probabilities with four different interpolation intervals of $N = 8, 16, 24, 32$: (a) $J_{tot} = 0$ and (b) $J_{tot} = 20$.

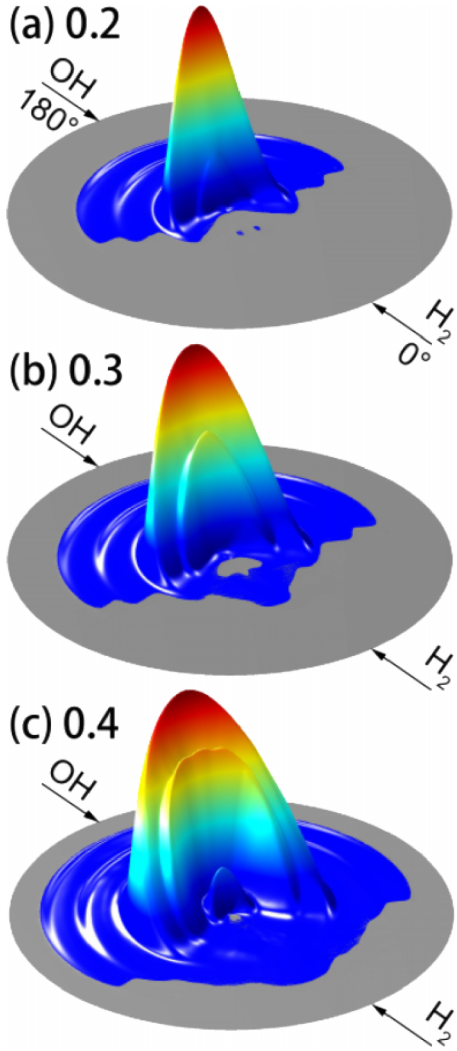

FIG. 5. Three-dimensional polar plots of the DCS at three collision energies of E_c: (a) 0.2 eV, (b) 0.3 eV, and (c) 0.4 eV. The radii of the three panels are in the same energy scale.

Figure 5 displays the three-dimensional polar plots of the state-to-state DCSs at three collision energies of $E_c = 0.2, 0.3$, and 0.4 eV. The DCSs are convoluted with a Gaussian width of 0.05 eV. These 3D DCSs represent the translational and angular distributions of the products. The maximum radii of the three panels are fixed at the same energy so that the relative translational energy is proportional to the radius. The angular distribution of the scattered H_2O product is relative to the incoming direction of the OH reactant. The forward direction of the H_2O product thus corresponds to 0° while backward direction to 180°. To plot the DCS in the full angle range (0°-360°), the part for (180°-360°) is duplicated from (0°-180°).

Consistent with the direct rebound reaction mechanism, all the DCSs are dominated by the backward direction. This is in agreement with the previous experimental and theoretical results on related reactions.[16–18,20,21,36,37,65–70] At the collision energy of $E_c = 0.2$ eV, the H_2O product is formed in the vibrational states with one quantum of stretching vibration in the newly formed OH bond. These states correspond to the large arc in Fig. 5(a). The outermost and second outermost

arcs with larger radii correspond to the ground and bending excited vibrational states of H_2O. At higher collision energies, $E_c = 0.3$ and 0.4 eV, the angular distribution extends to a large range and a shoulder arc adjacent to the highest arc emerges, which corresponds to the combined excitation of H_2O with one quantum of stretching and one quantum of bending vibration. At $E_c = 0.4$ eV, another vibrational state appears as an inner arc in Fig. 5(c), corresponding to two quanta of stretching vibration of H_2O. The pattern of vibrational excitation in the H_2O product is also consistent with the HD + OH → D + H_2O reaction studied before.[16,18] For example, at the collision energy of $E_c = 0.2$ and 0.3 eV, the H_2O product is mainly formed in the vibrational state with one quantum of stretching vibration, along with one extra quantum of bending vibration. The ground and bending fundamental states of the H_2O product are also observed but they are not very strong. At $E_c = 0.4$ eV, a negligible amount of H_2O from the HD + OH reaction[18] is formed in the states with two quanta of stretching vibration, while in H_2 + OH reaction such states are clearly seen as the small inner arc in Fig. 5(c). This can be presumably rationalized by noting the larger total energy in the latter case, as the H_2 reactant has more internal energy than HD reactant. On the other hand, the vibrational excitation of DOH product in the D_2 + OH reaction is quite different. The DOH with two quanta of OD stretching vibration is dominant.[17,20,65] The excitation of two quanta instead of one quantum OD stretching is determined by the transition state geometry and the internal energy of OD stretching vibration in the DOH product.

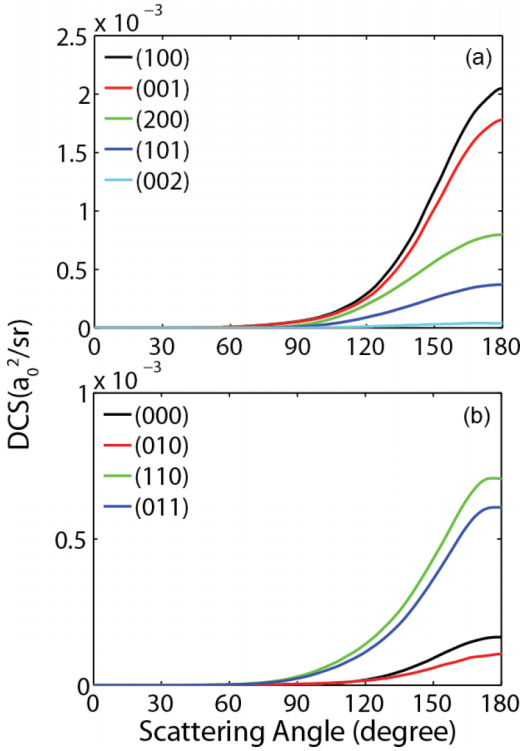

FIG. 6. Ro-vibrational state resolved DCS of the $H_2O(v_s v_b v_a, J' = 0)$ product at the collision energy of $E_c = 0.4$ eV. The numbers in $(v_s v_b v_a)$ represent the normal-mode quantum numbers of the symmetric stretching, bending, and anti-symmetric stretching modes of the H_2O product.

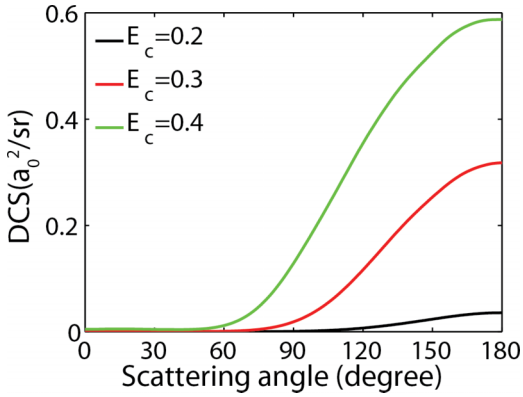

FIG. 7. Total DCSs with all the product state contribution summed together at three collision energies of $E_c = 0.2, 0.3$, and 0.4 eV.

To explicitly analyze the final vibrational state distribution of the H_2O product, the ro-vibrational state resolved DCSs at $E_c = 0.4$ eV are shown in Fig. 6. There exist a massive number of ro-vibrational states for the H_2O product and an accurate assignment of all the states is very challenging. Here, only the vibrational states of the H_2O product with $J' = 0$ are shown. Consistent with the above 3D plots of DCSs in Fig. 5, all the final state resolved DCSs are backward biased. The (100) and (001) states are the two dominant ones and the states with two quanta of stretching vibration are also observed, especially the (200) state. This is consistent with the observation in a previous study of the state-to-state mode specificity of the same reaction,[49] which can be explained by the sudden vector projection model.[8] The (110) and (011) states corresponding to the shoulder of the highest arc in Fig. 5(c) also have significant values. The DCSs of the (000) and (010) states are the two smallest ones.

The total DCSs at the three collision energies are shown in Fig. 7 with respect to the scattering angle, which are obtained by summing over the translational energy in the polar plots in Fig. 4. The backward scattering is very clear in the plot of total DCSs. With the increase of the collision energy, the cross sections increase significantly and the angular distribution also extends to a large range. These trends are also in good agreement with previous results.

IV. CONCLUSION

In this work, we present a new full-dimensional quantum reactive scattering algorithm for the calculation of the state-to-state DCSs for tetratomic reactive systems. This RCB method extracts the *S*-matrix elements by interpolating the time-dependent wave packet on the product coordinate grid at selected time intervals. This interpolation, while computationally demanding, avoids the massive storage of the product state wave packets. It differs from the RPD method in that no additional propagation is needed in the product channel. Hence, it should be able to handle reactions dominated by a post-transition state well or long-range interactions. Thus, the RCB method should be considered as an effective and general quantum mechanical scheme for extracting state-to-state information. The validity of the

method is confirmed here by the calculation of the state-to-state differential cross sections for the $H_2 + OH \rightarrow H + H_2O$ reaction. It opens the door for full-dimensional quantum mechanical calculations of the DCSs for more complicated tetratomic reactions such as $F + H_2O \rightarrow HF + OH$.

ACKNOWLEDGMENTS

This work was supported by the US Department of Energy (Grant No. DE-SC0015997 to H.G.) and by the National Natural Science Foundation of China (Grant Nos. 2013CB922200 and 21133006 to Z.S.). B.Z. would like to acknowledge support from the "Chunhui" program of Chinese Ministry of Education during his visit to Dalian Institute of Chemical Physics. The calculations were performed at the Center for Advanced Research Computing (CARC) at University of New Mexico.

[1]K. Liu, Annu. Rev. Phys. Chem. **52**, 139 (2001).
[2]M. Brouard, P. O'Keeffe, and C. Vallance, J. Phys. Chem. A **106**, 3629 (2002).
[3]X. Yang, Annu. Rev. Phys. Chem. **58**, 433 (2007).
[4]K. Liu, Annu. Rev. Phys. Chem. **67**, 91 (2016).
[5]S. C. Althorpe and D. C. Clary, Annu. Rev. Phys. Chem. **54**, 493 (2003).
[6]W. Hu and G. C. Schatz, J. Chem. Phys. **125**, 132301 (2006).
[7]G. Czakó and J. M. Bowman, J. Phys. Chem. A **118**, 2839 (2014).
[8]H. Guo and B. Jiang, Acc. Chem. Res. **47**, 3679 (2014).
[9]J. Li, B. Jiang, H. Song, J. Ma, B. Zhao, R. Dawes, and H. Guo, J. Phys. Chem. A **119**, 4667 (2015).
[10]D. H. Zhang and H. Guo, Annu. Rev. Phys. Chem. **67**, 135 (2016).
[11]H. Guo and K. Liu, Chem. Sci. **7**, 3992 (2016).
[12]M. A. Collins, Theor. Chem. Acc. **108**, 313 (2002).
[13]J. M. Bowman, G. Czakó, and B. Fu, Phys. Chem. Chem. Phys. **13**, 8094 (2011).
[14]B. Jiang, J. Li, and H. Guo, Int. Rev. Phys. Chem. **35**, 479 (2016).
[15]J. Z. H. Zhang, *Theory and Application of Quantum Molecular Dynamics* (World Scientific, Singapore, 1999).
[16]C. Xiao, X. Xu, S. Liu, T. Wang, W. Dong, T. Yang, Z. Sun, D. Dai, X. Xu, D. H. Zhang, and X. Yang, Science **333**, 440 (2011).
[17]S. Liu, C. Xiao, T. Wang, J. Chen, T. Yang, X. Xu, D. H. Zhang, and X. Yang, Faraday Discuss. **157**, 101 (2012).
[18]S. Liu, X. Xu, and D. H. Zhang, J. Chem. Phys. **136**, 144302 (2012).
[19]S. Liu and D. H. Zhang, Chem. Sci. **7**, 261 (2016).
[20]B. Zhao, Z. Sun, and H. Guo, J. Chem. Phys. **145**, 134308 (2016).
[21]Z. Zhao, S. Liu, and D. H. Zhang, J. Chem. Phys. **145**, 134301 (2016).
[22]S. K. Gray and G. G. Balint-Kurti, J. Chem. Phys. **108**, 950 (1998).
[23]S. Y. Lin and H. Guo, Phys. Rev. A **74**, 022703 (2006).
[24]M. Hankel, S. C. Smith, R. J. Allan, S. K. Gray, and G. G. Balint-Kurti, J. Chem. Phys. **125**, 164303 (2006).
[25]W. Zhu, J. Dai, J. Z. H. Zhang, and D. H. Zhang, J. Chem. Phys. **105**, 4881 (1996).
[26]D. H. Zhang and J. C. Light, J. Chem. Phys. **105**, 1291 (1996).
[27]D. H. Zhang, D. Xie, and M. Yang, Phys. Rev. Lett. **89**, 283203 (2002).
[28]D. H. Zhang, J. Chem. Phys. **125**, 133102 (2006).
[29]S. Gómez-Carrasco and O. Roncero, J. Chem. Phys. **125**, 054102 (2006).
[30]Z. Sun, X. Lin, S.-Y. Lee, and D. H. Zhang, J. Phys. Chem. A **113**, 4145 (2009).
[31]Z. Sun, H. Guo, and D. H. Zhang, J. Chem. Phys. **132**, 084112 (2010).
[32]B. Zhao, Z. Sun, and H. Guo, J. Chem. Phys. **144**, 064104 (2016).
[33]T. Peng and J. Z. H. Zhang, J. Chem. Phys. **105**, 6072 (1996).
[34]S. C. Althorpe, D. J. Kouri, and D. K. Hoffman, J. Chem. Phys. **107**, 7816 (1997).
[35]S. C. Althorpe, J. Chem. Phys. **114**, 1601 (2001).
[36]M. T. Cvitaš and S. C. Althorpe, J. Phys. Chem. A **113**, 4557 (2009).
[37]M. T. Cvitaš and S. C. Althorpe, Phys. Scr. **80**, 048115 (2009).
[38]J. Li, R. Dawes, and H. Guo, J. Chem. Phys. **137**, 094304 (2012).
[39]R. Otto, J. Ma, A. W. Ray, J. S. Daluz, J. Li, H. Guo, and R. E. Continetti, Science **343**, 396 (2014).
[40]J. Ma and H. Guo, J. Phys. Chem. Lett. **6**, 4822 (2015).
[41]P. F. Conforti, M. Braunstein, B. J. Braams, and J. M. Bowman, J. Chem. Phys. **133**, 164312 (2010).
[42]J. Li and H. Guo, J. Chem. Phys. **138**, 194304 (2013).
[43]J. Li, R. Dawes, and H. Guo, Phys. Chem. Chem. Phys. **18**, 29825 (2016).
[44]Z. Sun, S.-Y. Lee, H. Guo, and D. H. Zhang, J. Chem. Phys. **130**, 174102 (2009).
[45]R. Welsch, F. Huarte-Larrañaga, and U. Manthe, J. Chem. Phys. **136**, 064117 (2012).
[46]U. Manthe and R. Welsch, J. Chem. Phys. **140**, 244113 (2014).
[47]B. Zhao, Z. Sun, and H. Guo, J. Chem. Phys. **140**, 234110 (2014).
[48]B. Zhao, Z. Sun, and H. Guo, J. Chem. Phys. **141**, 154112 (2014).
[49]B. Zhao, Z. Sun, and H. Guo, J. Am. Chem. Soc. **137**, 15964 (2015).
[50]U. Manthe and R. Ellerbrock, J. Chem. Phys. **144**, 204119 (2016).
[51]B. Zhao and H. Guo, J. Phys. Chem. Lett. **6**, 676 (2015).
[52]B. Zhao, Z. Sun, and H. Guo, J. Chem. Phys. **142**, 241101 (2015).
[53]B. Zhao, Z. Sun, and H. Guo, J. Chem. Phys. **144**, 214303 (2016).
[54]H. Wei and T. Carrington, Jr., J. Chem. Phys. **97**, 3029 (1992).
[55]J. Echave and D. C. Clary, Chem. Phys. Lett. **190**, 225 (1992).
[56]D. T. Colbert and W. H. Miller, J. Chem. Phys. **96**, 1982 (1992).
[57]D. H. Zhang and J. Z. H. Zhang, J. Chem. Phys. **99**, 5615 (1993).
[58]R. N. Zare, *Angular Momentum* (Wiley, New York, 1988).
[59]D. H. Zhang and J. Z. H. Zhang, J. Chem. Phys. **101**, 1146 (1994).
[60]D. H. Zhang and J. C. Light, J. Chem. Phys. **104**, 4544 (1996).
[61]J. Dai and J. Z. H. Zhang, J. Phys. Chem. **100**, 6898 (1996).
[62]W. Yang and A. C. Peet, Chem. Phys. Lett. **153**, 98 (1988).
[63]Z. Sun, W. Yang, and D. H. Zhang, Phys. Chem. Chem. Phys. **14**, 1827 (2012).
[64]W. Li, D. H. Zhang, and Z. Sun, J. Phys. Chem. A **118**, 9801 (2014).
[65]B. R. Strazisar, C. Lin, and H. F. Davis, Science **290**, 958 (2000).
[66]J. Espinosa-García, L. Bonnet, and J. C. Corchado, Phys. Chem. Chem. Phys. **12**, 3873 (2010).
[67]J. D. Sierra, L. Bonnet, and M. González, J. Phys. Chem. A **115**, 7413 (2011).
[68]J. D. Sierra, R. Martinez, J. Hernando, and M. González, Phys. Chem. Chem. Phys. **11**, 11520 (2009).
[69]M. T. Cvitaš and S. C. Althorpe, J. Chem. Phys. **134**, 024309 (2011).
[70]M. T. Cvitaš and S. C. Althorpe, J. Chem. Phys. **139**, 064307 (2013).
[71]J. Chen, X. Xu, X. Xu, and D. H. Zhang, J. Chem. Phys. **138**, 154301 (2013).
[72]M. D. Feit, J. A. Fleck, Jr., and A. Steiger, J. Comput. Phys. **47**, 412 (1982).
[73]H. Guo, Rev. Comput. Chem. **25**, 285 (2007).
[74]S. C. Althorpe, D. J. Kouri, and D. K. Hoffman, J. Chem. Phys. **106**, 7629 (1997).